JACS
JOURNAL OF THE AMERICAN CHEMICAL SOCIETY
Article
pubs.acs.org/JACS

Nanosecond Time Scale Motions in Proteins Revealed by High-Resolution NMR Relaxometry

Cyril Charlier,[†,⊥] Shahid Nawaz Khan,[†,⊥] Thorsten Marquardsen,[‡] Philippe Pelupessy,[†] Volker Reiss,[‡] Dimitris Sakellariou,[†,§] Geoffrey Bodenhausen,[†,∥] Frank Engelke,[‡] and Fabien Ferrage*[,†]

[†]Laboratoire des Biomolécules, Département de Chimie, UMR 7203 CNRS-UPMC-ENS, Ecole Normale Supérieure, 24 Rue Lhomond, 75231 Paris Cedex 05, France

[‡]Bruker BioSpin GmbH, Silberstreifen 4, D 76287 Rheinstetten, Germany

[§]Laboratoire Structure et Dynamique par Résonance Magnétique, UMR 3299-SIS2M CEA/CNRS, IRAMIS, DSM, CEA Saclay, F-91191, Gif-sur-Yvette Cedex, France

[∥]Institut des Sciences et Ingénierie Chimiques, Ecole Polytechnique Fédérale de Lausanne, BCH, 1015 Lausanne, Switzerland

Supporting Information

ABSTRACT: Understanding the molecular determinants underlying protein function requires the characterization of both structure and dynamics at atomic resolution. Nuclear relaxation rates allow a precise characterization of protein dynamics at the Larmor frequencies of spins. This usually limits the sampling of motions to a narrow range of frequencies corresponding to high magnetic fields. At lower fields one cannot achieve sufficient sensitivity and resolution in NMR. Here, we use a fast shuttle device where the polarization builds up and the signals are detected at high field, while longitudinal relaxation takes place at low fields $0.5 < B_0 < 14.1$ T. The sample is propelled over a distance up to 50 cm by a blowgun-like system in about 50 ms. The analysis of nitrogen-15 relaxation in the protein ubiquitin over such a wide range of magnetic fields offers unprecedented insights into molecular dynamics. Some key regions of the protein feature structural fluctuations on nanosecond time scales, which have so far been overlooked in high-field relaxation studies. Nanosecond motions in proteins may have been underestimated by traditional high-field approaches, and slower supra-τ_c motions that have no effect on relaxation may have been overestimated. High-resolution relaxometry thus opens the way to a quantitative characterization of nanosecond motions in proteins.

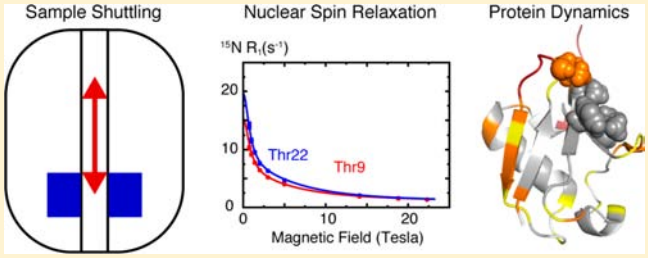

INTRODUCTION

The chemical and physical principles underlying protein function can only be unraveled by gaining insight into both structural and dynamic features. Nuclear magnetic resonance spectroscopy is unmatched in its ability to provide such insight at atomic resolution. Nuclear spin relaxation, i.e., the return of the perturbed magnetization to its equilibrium, allows one to characterize internal protein dynamics in two distinct ranges: fast pico- to nanosecond and slow micro- to millisecond time scales.[1] Overall rotational diffusion of proteins, which occurs typically on time scales τ_c on the order of a few nanoseconds to several tens of nanoseconds, and internal motions on time scales $\tau_{int} \lesssim \tau_c$ lead to stochastic fluctuations of orientation-dependent spin interactions such as dipole−dipole couplings and anisotropic chemical shifts. The resulting relaxation rates depend on spectral density functions $J(\omega)$, which are defined as Fourier transforms of the correlation functions $C(t)$ of the orientation-dependent interactions. The measurement of a series of relaxation rates allows one to "map" the spectral density functions $J(\omega)$,[2] thus providing quantitative parameters for models of overall and internal motions. Most models employed to date rely on the hypothesis that internal motions are statistically independent of the rotational diffusion of a macromolecule, which is usually justified by the separation of the time scales of overall and internal motions, the latter being hitherto considered to be at least an order of magnitude faster than the former.[3] Internal motions are usually described by one or two order parameters and discrete internal correlation times[4,5] or by a distribution of such internal correlation times.[6−8] The hypothesis that the time scales of overall and local motions can be separated and that they are statistically independent has however been challenged.[9] The discrimination between different models of motions has proven to be difficult because the spectral density functions could only be properly determined over few narrow ranges of fairly high frequencies. This limitation can be overcome by "relaxometry", i.e., by measuring relaxation rates over a wide range of magnetic fields, typically from 1 μT to 3 T. So far, this could only be achieved at the expense of sensitivity and resolution.[10,11] Relaxometry can

Received: September 26, 2013
Published: November 14, 2013

   dx.doi.org/10.1021/ja409820g | J. Am. Chem. Soc. 2013, 135, 18665−18672

be reconciled with high-resolution high-field NMR by rapidly "shuttling" the sample from high to low field and back.[12−14] Slower shuttling has allowed fruitful studies of slowly relaxing phosphorus-31 and carbon-13 nuclei in lipids,[15] but relaxation of nitrogen-15 in proteins is so fast at low fields that the shuttling must be carried out very rapidly. To the best of our knowledge, there is only one pioneering study,[16] albeit shuttling was limited to a fairly narrow range of magnetic fields (down to 4 T).

Here, we use high-resolution relaxometry combined with traditional high-field measurements to measure relaxation rates over nearly 2 orders of magnitude (0.5−22.3 T.) We illustrate the power of this method by revealing internal nanosecond-time scale dynamics in the protein ubiquitin. (Poly)-ubiquitination is a mechanism involved in many biological cell-signaling processes, from protein degradation to DNA damage response. Signaling is mediated by interactions of ubiquitin and polyubiquitin with a broad range of protein partners. Such a diversity is made possible through the conformational flexibility of its 76 amino acid chain.[17] This observation was highlighted in a recent study[18] where the internal dynamics of ubiquitin were modified to bind selectively to a single partner, primarily by reducing the flexibility of its $\beta_1-\beta_2$ turn (residues 7−13).

It has been shown that the intrinsic flexibility of ubiquitin in its free apo form leads to a rich conformational landscape, which is similar to the conformational diversity in ubiquitin complexes.[19] Binding to a given partner can be described by an induced fit, a conformational selection, or an intermediate mechanism, depending on the time scales of conformational transitions and the lifetimes of encounter complexes.[20] Unraveling the time scales of internal motions in ubiquitin is obviously a prerequisite to understanding the kinetic pathways of binding reactions. Many NMR studies have sought to identify signatures of chemical exchange in ubiquitin in solution,[21−25] demonstrating the presence of internal motions on slow time scales ($10 \lesssim \tau_{int} \lesssim 100$ μs). Residual dipolar couplings (RDCs)[26−30] also point to the presence of extensive slow supra-τ_c time scales of 5 ns $\lesssim \tau_{int} \lesssim$ 10 ms (with $\tau_c \approx 5$ ns), which could not be detected by high-field relaxation or by chemical exchange phenomena. Several studies of faster sub-τ_c motions with $\tau_{int} \lesssim \tau_c = 5$ ns have been carried out using ^{15}N or ^{13}C relaxation.[31−34] Most of these studies rely on data acquired at a single high magnetic field and use simple spectral density functions. The results are often compared to those derived from RDC measurements, and discrepancies are attributed to contributions of supra-τ_c motions. We show that high-resolution relaxometry can reveal a surprising complexity of internal protein motions with time scales comparable to overall tumbling that were overlooked in high-field relaxation studies. We show that slower supra-τ_c motions have likely been overestimated so far, in particular in the essential extended $\beta_1-\beta_2$ turn.

RESULTS AND DISCUSSION

The sensitivity of relaxometry to motions on nanosecond time scales is illustrated in Figure 1. We have simulated the longitudinal relaxation rates of nitrogen-15 at several magnetic fields, assuming motions over a range of time scales and amplitudes. An extended model-free[5] spectral density function was assumed with variable order parameters and time scales for slow motions on nanosecond time scales. Analytical expressions can be found in the Supporting Information. The longitudinal

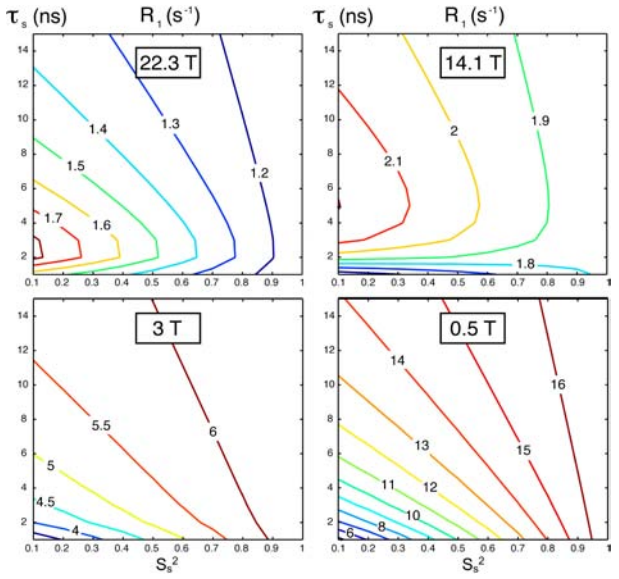

Figure 1. Simulated dependence of longitudinal nitrogen-15 relaxation rates on internal motions with nanosecond time scales, i.e., below and above the correlation time for overall tumbling $\tau_c = 5$ ns. An extended model-free spectral density function was used with the following parameters: $\tau_c = 5$ ns; correlation time for fast internal motions $\tau_{fast} = 10$ ps; order parameters for fast internal motions $S^2_{fast} = 0.8$; order parameters for slow internal motions $0.1 < S^2_{slow} < 1.0$ (x axis); 1 ns $< \tau_{int} < 15$ ns (y axis).

relaxation rates vary strongly with the magnetic field, depending on the parameters of local motions. Both high- and low-field relaxation rates are remarkably sensitive to slow sub-τ_c motions if the order parameters are low. The rates at low fields are more sensitive to internal motions when their correlation times are comparable to the overall tumbling time. Relaxation rates at 0.5 T are more sensitive to internal motions than those recorded at 3 T, which underscores the advantages of studying relaxation at low magnetic fields. Longitudinal relaxation rates are largely insensitive to internal motions with slow time scales $\tau_{int} \gtrsim \tau_c/2$ at 14.1 T, i.e., at high magnetic fields where many studies of internal dynamics in ubiquitin have been carried out so far. The different patterns for the dependence of longitudinal relaxation rates at high and low fields underline the enhanced sensitivity to nanosecond motions of relaxation measurements over a broad range of magnetic fields.

We developed a pneumatic system for fast shuttling, based on a system that was originally developed for liquid-state dynamic nuclear polarization (DNP) studies where the proton polarization observed at 14.1 T can be enhanced by saturating EPR transitions at 0.34 T.[35] Our shuttle consists of a custom-designed probe (Figure 2a,b), a transfer system, and a control unit, as described in more detail in Supporting Information. The probe uses two saddle coils, like in standard high-resolution probes. The inner coil is doubly tuned for ^{13}C and ^{15}N, while the orthogonal outer coil is doubly tuned for ^{1}H and ^{2}H. This reduces interactions between the sample and the electric component of the rf field, albeit at the expense of a slight loss of sensitivity. The design affords a spectral resolution and line shapes comparable to those obtained using state-of-the-art high-resolution probes at 600 MHz. Special care was taken (Figure 2a) to reduce vibrations arising from the abrupt "landing" of the shuttle at the lower end (see Supporting Information). A long tube guides the shuttle during its motion

dx.doi.org/10.1021/ja409820g | J. Am. Chem. Soc. 2013, 135, 18665−18672

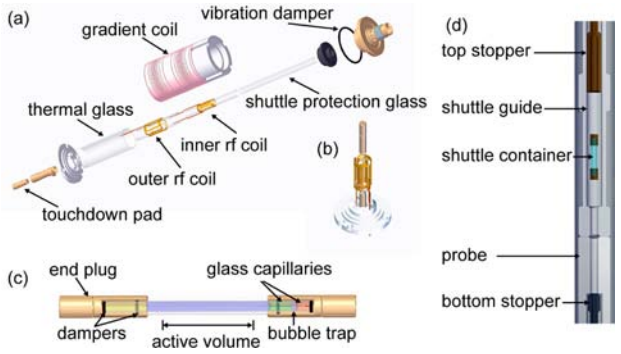

Figure 2. Schematic views of the fast shuttling system: (a) expanded view of the upper part of the probe; (b) coil assembly with shuttle container; (c) shuttle container; (d) schematic view (not to scale) of the full assembly in the bore of a high-field magnet.

(Figure 2c). The upper position of the shuttle is controlled by an adjustable inner tube. The inner tube is connected to the guiding tube by another damping system to reduce vibrations.

A special quartz container was chosen for protein samples (Figure 2d). Synthetic amorphous quartz glass with a low magnetic susceptibility can resist a large number of shocks. (A single container was used for more than 500 000 shuttling events in the course of this study.) In the shuttle container, a ~100 μL sample compartment is separated from a ~10 μL "bubble catcher" compartment by a narrow capillary (150 μm inner diameter). Bubbles appearing in the course of extensive experimental series can be centrifuged into the bubble catcher before resuming the experiments. The active volume that lies within the rf coils is 60 μL (Figure 2d). The resulting sensitivity of this system is about an order of magnitude lower than the sensitivity of a room-temperature TXI probe used with a large-volume sample. This currently limits applications to the study of (bio)molecules that have a good solubility or favorable relaxation properties.

We used this shuttling system to measure the longitudinal relaxation of backbone nitrogen-15 nuclei in uniformly nitrogen-15 labeled human ubiquitin in acetate buffer at pH 4.5 and T = 296.6 ± 0.6 K. The pulse sequence used for these measurements is shown in Figure 3. After a recovery delay in high field (B_0^{high} = 14.1 T) to allow the Boltzmann polarization to build up, the temperature to be regulated, and the field-frequency lock to stabilize the field, the longitudinal polarization N_z of nitrogen-15 is enhanced using the refocused INEPT method.[36,37] The sample is then transferred in 41 < τ_{up} < 54 ms to a predetermined position in the stray field 27 < z < 46 cm above the magnetic center. The polarization is then allowed to relax in a low field B_0^{low} for a duration T_{rel} and transferred back to high field B_0^{high} in 40 < τ_{down} < 70 ms. During a stabilization delay τ_{st} = 100 ms, convection and vibrations are allowed to settle. Finally, the longitudinal nitrogen-15 polarization N_z is converted back into transverse proton magnetization for detection. The average signal-to-noise ratios in two-dimensional (2D) spectra obtained for the shortest relaxation delays T_{rel} = 39 ms were S/N = 66 at B_0^{low} = 5 T (at z = 27 cm above the magnetic center) and S/N = 24 for T_{rel} = 51 ms at B_0^{low} = 0.5 T (z = 46 cm) when 16 transients were recorded for each of 64 complex points in the indirect t_1 dimension (the experimental time was 85 min for each interval T_{rel}).

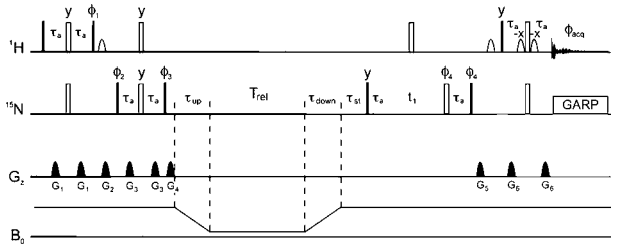

Figure 3. Pulse sequence for the measurement of longitudinal nitrogen-15 relaxation of amide nitrogen nuclei in proteins at various low fields B_0^{low} and recovery and detection at high field B_0^{high}. Narrow (filled) and wide (open) rectangles represent 90° and 180° pulses, respectively. Pulse phases are along the x-axis of the rotating frame unless otherwise specified. The bell-shaped pulses represent 1.2 ms sinc pulses. All delays τ_a are set to $1/|4J_{NH}|$, with J_{NH} = −92 Hz. The stabilization delay τ_{st} = 100 ms allows for convection currents and vibrations to settle. Pulsed field gradients G_z have smoothed rectangular amplitude profiles and 1 ms durations. Their peak amplitudes are G_1 = 25, G_2 = 40, G_3 = 11.5, G_4 = 20.5, G_5 = 40, G_6 = 15 G cm^{-1}. The phase cycles were $\varphi_1 = \{y, y, y, y, -y, -y, -y, -y\}$; $\varphi_2 = \{x, -x\}$; $\varphi_3 = \{y, y, y, y, y, y, y, y, -y, -y, -y, -y, -y, -y, -y, -y\}$; $\varphi_4 = \{x, x, -x, -x\}$; $\varphi_{acq} = \{x, -x, -x, x, -x, x, x, -x, -x, x, x, -x, x, -x, -x, x\}$.

Longitudinal relaxation rates were recorded at 7 different low magnetic fields. Each measurement was repeated 2 or 3 times. In addition, a full set of conventional nitrogen-15 relaxation experiments was recorded without shuttling at 14.1, 18.8, and 22.3 T (600, 800, and 950 MHz for ^{1}H) using state-of-the-art methods to cancel cross-correlation effects.[38−41] The parameters of rotational diffusion were derived from relaxation rates using the program ROTDIF.[42] Diffusion tensors obtained at all three high fields are virtually identical (see Supporting Information). On the basis of a solution-state structure of ubiquitin (PDB code 1d3z),[43] we obtained an axially symmetric diffusion tensor with $D_\parallel/D_\perp$ = 1.18 ± 0.08 and an overall correlation time $\tau_c = (6\mathrm{Tr}(\mathbf{D}))^{-1}$ = 4.84 ± 0.2 ns, where $\mathrm{Tr}(\mathbf{D})$ is the trace of the diffusion tensor from our measurements at 18.8 T. At a lower concentration (200 μM) at 14.1 T we found a slightly shorter overall correlation time τ_c = 4.22 ± 0.15 ns. The small variation of τ_c and the fact that the anisotropy and orientation of the diffusion tensor were found to be independent of concentration (see Supporting Information) suggest that the protein is in monomeric form at pH 4.5 and not in a monomer/dimer equilibrium, as found at neutral pH.[44] In our case, the low pH leads to the protonation of His68 and is likely to reduce the binding affinity of symmetric dimers that associate at the hydrophobic patch at neutral pH, as shown in diubiquitin.[45] Therefore, we believe that the slight increase of the overall correlation time τ_c was due to nonspecific intermolecular interactions at high concentration so that we could describe the overall rotational diffusion by a single time-independent tensor.

Particular care has been taken to control the temperature in these experiments, since temperature regulation at low field B_0^{low} is not yet feasible in our prototype. We have measured differences of chemical shifts between subsets of signals and calibrated them as a function of temperature.[23] The actual sample temperature was then derived from these chemical shift differences in each experiment. Only experiments with 296 ≤ T ≤ 297.2 K were retained in the analysis so that systematic errors can be safely neglected (see Supporting Information). Conventional high field-relaxation measurements at 14.1 and

dx.doi.org/10.1021/ja409820g | J. Am. Chem. Soc. 2013, 135, 18665−18672

18.8 T were carried out at 296.5 K. Rates measured at 22.3 T and 298.5 K were corrected to account for the change in τ_c.

The longitudinal relaxation rates $R_1(B_0) = 1/T_1(B_0)$ of ^{15}N nuclei in the backbone of ubiquitin determined at 10 different fields are shown in Figure 4. Cross-relaxation pathways lead to multiexponential decays, which in high fields can usually be transformed into monoexponential decays by suitable pulse sequences.[46,47] Since in our prototype it is not possible to apply any rf pulses in low fields, systematic deviations from monoexponential decays must be taken into account in the analysis.[16] We have developed a protocol dubbed "iterative correction for the analysis of relaxation under shuttling" (ICARUS). First, the analysis of relaxation rates was carried out (in terms of overall tumbling and microdynamics) at all three high fields 14.1, 18.8, and 22.3 T using the programs ROTDIF[42] and DYNAMICS.[48] The parameters resulting from this initial step were then used to predict the deviations from simple exponential decays in a spin system that comprises one ^{15}N−^{1}H pair and two remote protons (see Supporting Information). For each field B_0^{low}, we simulated the relaxation of each ^{15}N−^{1}H pair in ubiquitin *during* shuttling, with constant velocity (see Supporting Information). The deviations between the calculated "apparent" nitrogen-15 relaxation rates and the "true" low-field relaxation rates were then used to correct for systematic errors in the experimental rates. In a second iteration, longitudinal relaxation rates at all 10 fields and ^{15}N{^{1}H} NOEs at the three high fields 14.1, 18.8, and 22.3 T were used as input to the program DYNAMICS. This cycle was reiterated four times to achieve a satisfactory convergence for all residues. The typical corrections varied from 4.5% to 13%. Cross-correlations of the fluctuations of nitrogen-15 chemical shift anisotropies and ^{15}N−^{1}H dipolar couplings are dominant above 3 T, with average corrections ranging from 5.1% at 3 T to 9.2% at 5 T, while ^{15}N−^{1}H dipolar cross-relaxation dominates below 2 T, with corrections on the order of 11% at fields below 1 T.

The results of this analysis are shown in Figure 5. As expected from studies of ^{15}N and ^{13}C relaxation,[31,32] residual

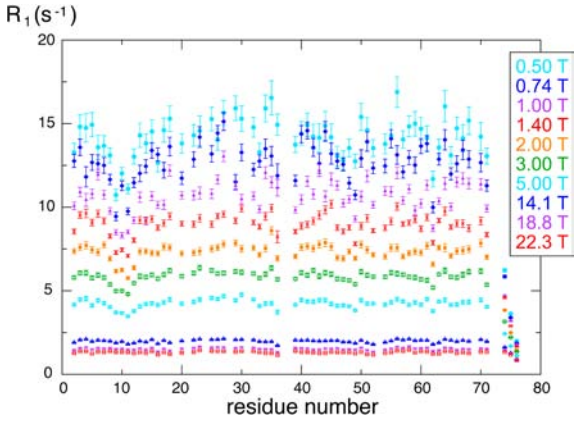

Figure 4. Experimental longitudinal relaxation rates $R_1 = 1/T_1$ of ^{15}N in backbone amide groups of ubiquitin as a function of magnetic fields $0.5 \le B_0^{low} \le 5$ T and $14.1 \le B_0^{high} \le 22.3$ T. From bottom to top: B_0^{high} = 22.3, 18.8, 14.1 (red squares, magenta crosses, blue triangles); B_0^{low} = 22.3, 18.8, 14.1 5.0, 3.0, 2.0, 1.4, 1.0, 0.74, and 0.5 T (cyan diamonds, green circles, orange squares, red crosses, magenta triangles, blue diamonds, cyan circles). Note that all rates increase with decreasing field. The lower B_0^{low} is, the greater are the variations of the rates along the backbone.

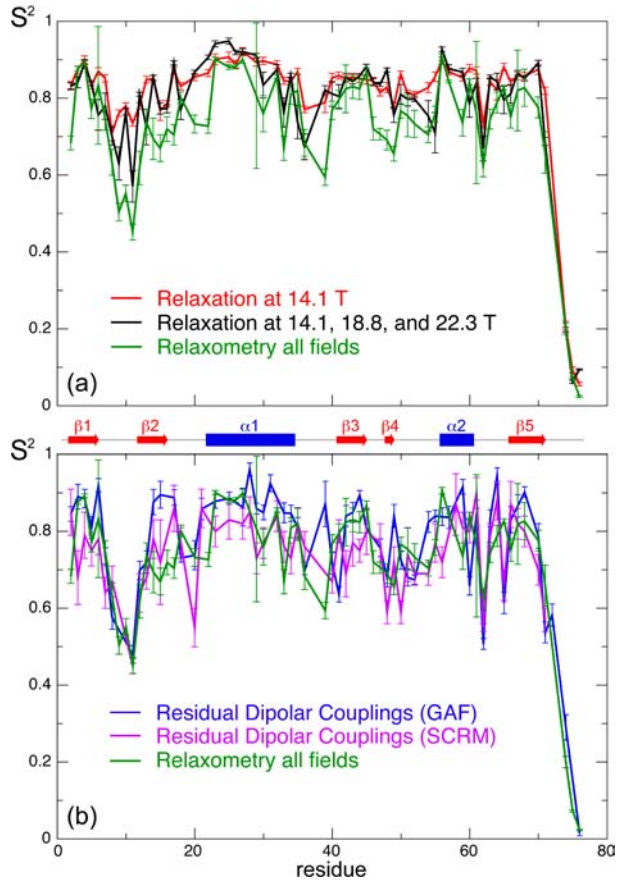

Figure 5. (a) Order parameters S^2 in ubiquitin obtained from the analysis of nitrogen-15 relaxation rates, taking into account (red) relaxation rates at 14.1 T only; (black) relaxation data at three fields 14.1, 18.8, and 22.3 T; (green) relaxation rates at all 10 fields from 0.5 to 22.3 T. (b) Comparison of order parameters obtained from relaxation rates at all fields (green) and from analysis of residual dipolar couplings (RDCs) in large sets of orienting media, either by GAF (blue)[30] or SCRM (purple).[28]

dipolar couplings,[26,28,29] and molecular dynamics,[49−51] we find that ubiquitin is fairly rigid. However, we determined the order parameters to be significantly lower than in earlier relaxation-based studies. We may compare (Figure 4) (i) the order parameters resulting from all 10 fields, (ii) those obtained from relaxation rates at 14.1 T only, and (iii) those obtained at three high fields (14.1, 18.8, and 22.3 T). With few exceptions, the order parameters resulting from our analysis of relaxation at 10 magnetic fields are the lowest. In particular, the dynamics of the crucial β_1−β_2 turn (residues 7−12) can be best described by an extended model-free[5] spectral density function with similar time scales for all six residues (see Supporting Information). A global fit of these six residues gives a common effective time scale τ_{7-12} = 2 ns. This is in good agreement with the well-documented hypothesis of a collective motion.[52] This motion was so far believed to occur on a much slower, so-called supra-τ_c time scale $\tau_{7-12} > \tau_c$, since RDC studies indicated large-amplitude motions while relaxation at a single high field failed to detect such motions. Interestingly, lower order parameters and motions on similar time scales (see Supporting Information) are also found at the C-terminus of helix α_1 and loop α_1−β_4 (residues 33 and 36), which participate, along with the β_1−β_2 turn, in the principal mode of ubiquitin dynamics.[19,53] The relaxation of this principal mode could be

dx.doi.org/10.1021/ja409820g | J. Am. Chem. Soc. 2013, 135, 18665−18672

described in silico with two time scales, 0.4 and 13 ns.[53] Our analysis assumes only one single time scale for the semilocal motions, and the fit leads to an intermediate value, τ_{7-12} = 2 ns, which could well result from effective averaging between these two time scales. More complex models of spectral density functions should open the way to a better agreement between experimental rates and theory.

The inability of high-field relaxation studies to identify these motions is hardly surprising, since most studies have only been carried out at a single field. Therefore, the sampling of the spectral density function was insufficient and did not characterize sufficiently well motions on nanosecond time scales. The consequences of undersampling of the spectral density function are exacerbated if one uses simple models that do not properly reproduce the actual spectral density functions. Strikingly, the order parameters for fast motions obtained by extended-model free analysis of all relaxation rates match very well with order parameters obtained from the analysis of relaxation data at 14.1 T only (see Supporting Information). This point is also nicely illustrated by the analysis of a 1.2 μs molecular dynamics trajectory of ubiquitin.[50] In this study, order parameters S^2 derived from the average orientations of NH vectors were low for the $\beta_1-\beta_2$ turn. However, when the nonexponential correlation functions were forced to fit with a simple extended model-free correlation function, the order parameters became significantly higher, similar to those found in relaxation studies at 14.1 T.[32]

Figure 5b presents the comparison of orders parameters obtained (i) from our relaxometry analysis of relaxation at 10 magnetic fields and (ii) from two independent analyses of residual dipolar couplings (RDCs) in large sets of oriented media using the Gaussian axial fluctuations (GAF)[30] or the self-consistent RDC-based model-free analysis (SCRM)[28] approaches. The three profiles are similar. In particular, the order parameters in the $\beta_1-\beta_2$ turn (residues 7−12) are almost identical so that one expects the amplitudes of motions in this turn that cannot be detected by relaxation to be very small. Significant correlations between slow supra-τ_c motions of the $\beta_1-\beta_2$ turn and those of the β sheet are therefore unlikely, although correlated motions in the core of the β-sheet cannot be excluded.[52] Our relaxometry data show that the whole β_2 strand, which lies at the edge of the β-sheet, is significantly dynamic. Similarly, studies of the third immunoglobin binding domain of streptococcal protein G (GB3) have also shown the presence of enhanced motions in the last strand of an otherwise fairly rigid β-sheet.[54] These results differ from those of a GAF analysis of dynamics in ubiquitin,[29] where the β_2-strand is found to be rigid. However, they are in better agreement with results from the SCRM analysis.[28]

In addition to this region, our relaxometry method allowed us to detect enhanced dynamics in several loops: $\beta_2-\alpha_1$, $\beta_4-\alpha_2$, and $\alpha_2-\beta_5$ as well as in the $\beta_3-\beta_4$ turn and β_4 strand, which lies at the opposite edge of the β sheet. This is, again, in good qualitative agreement with both RDC studies (see Figure 5b). The agreement with accelerated molecular dynamics simulations is excellent, with a good correlation coefficient (R = 0.91) between the two data sets (see Supporting Information). Note, however, that the order parameters found by relaxometry are systematically (albeit only slightly) lower than those obtained by molecular dynamics.

Figure 6 shows a graphical representation of order parameters in ubiquitin. The edges of the β-sheet are occupied by the $\beta_1-\beta_2$ turn and the flexible C-terminal tail at one end

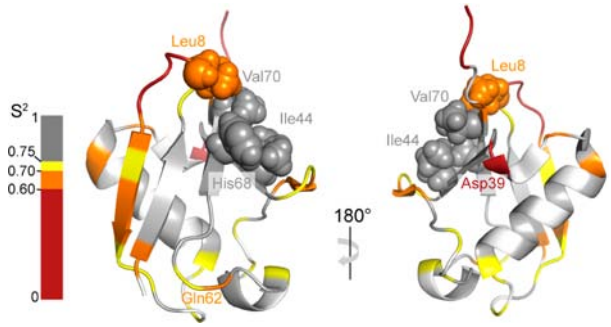

Figure 6. Large amplitude dynamics in ubiquitin on fast nanosecond time scales. Rigid residues with high order parameters $S^2 > 0.75$ are shown in gray. Mobile residues with intermediate and small order parameters are shown in yellow ($0.70 < S^2 < 0.75$), orange ($0.60 < S^2 < 0.70$), and red ($S^2 < 0.6$.). Residues for which no data are available are shown in white. The main interface with binding partners comprises the side chains of residues Leu8, Ile44, His68, and Val70 represented by space-filling models.

and by the $\alpha_2-\beta_5$ loop and $\beta_3-\beta_4$ turn at the other end, with the β_2 and β_4 strands on each side. All of these regions are found to be dynamic, albeit to different extent. The picture that emerges is a hierarchy of time scales[55] near the main binding interface of ubiquitin that consists of a β-sheet with a core that is flexible on a slow time scale of about 50 μs,[23,25] while its edges are mobile on faster nanosecond time scales. Between these two time scales, small correlated fluctuations of the β-sheet also appear to be allowed.[52] The ability of the edges of the interface to undergo conformational rearrangements on nanosecond time scales would be compatible with an induced fit mechanism in the early stage of binding.

Figure 7 shows a few selected plots of longitudinal relaxation rates $R_1(B_0)$. Dramatic differences can be observed between mobile and rigid residues. A good agreement between experimental and theoretical profiles is observed for most residues. Some dispersion profiles feature systematic discrepancies, which highlight the limitations of current models of

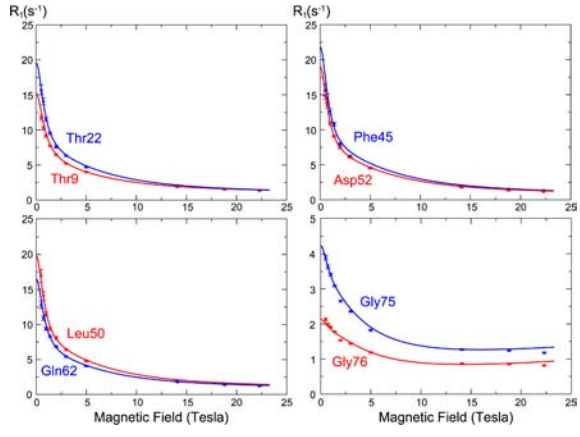

Figure 7. Longitudinal relaxation rates $R_1(B_0)$ as a function of the static field (so-called "relaxometry dispersion profiles") for eight selected residues in ubiquitin. Note that the vertical scale is expanded by a factor of 5 for the two C-terminal glycines (bottom right). The blue and red dots show corrected longitudinal relaxation rates, adjusted to compensate for relaxation during shuttling, while the lines show dispersion profiles calculated from the microdynamic parameters obtained in our analysis.

dx.doi.org/10.1021/ja409820g | J. Am. Chem. Soc. 2013, 135, 18665−18672

spectral density functions. Our experimental data call for the development of new, more sophisticated models. Some relaxation profiles, e.g., for the highly mobile C-terminal glycine residues G75 and G76, present deviations from the theoretical profiles at both high and low magnetic fields, even when postulating a spectral density function comprising a sum of three Lorentzian functions with five adjustable parameters, thus suggesting the presence of a distribution of time scales.[8] In particular, with only two time scales for internal motions, the fitted spectral density function is rather flat at high frequencies. Hence, contributions of the chemical shift anisotropy to relaxation lead to an increase in the $R_1(B_0)$ curve between 14 and 23 T, in contradiction with experimental results. Similarly, a small but systematic underestimation of the spectral density $J(\omega=0)$ in some of the most mobile regions, and hence of the back-predicted transverse relaxation rates (see Supporting Information), can be understood by postulating a rapid initial decay of the spectral density function at low frequencies. Interestingly, no significant contribution of chemical exchange to transverse relaxation R_{ex} could be detected (see Supporting Information).[39,56] The analysis of relaxation at three high fields also leads to underestimate $J(\omega=0)$, as illustrated by the need for urealistic R_{ex} contributions to fit *all* relaxation data. Nanosecond fluctuations of the overall diffusion tensor associated with motions of the C-terminal tail, transient oligomerization,[10] and mode coupling of local and global motions[9,57,58] may be responsible for these unexpected features.

We have measured and analyzed residue-specific relaxation rates in a protein over a range of nearly 2 orders of magnitude of magnetic fields. Our high-resolution relaxometry approach reveals unexpected motions in the protein ubiquitin. In particular, the motion of the $\beta_1-\beta_2$ turn appears to have larger amplitudes than could be previously identified by relaxation at high fields, in agreement with RDCs and MD. Until now, discrepancies between high-field relaxation and RDC-based methods were attributed to the cutoff of internal motions by overall rotation. High-field relaxation studies have led to underestimate sub-τ_c and near-τ_c motions because relaxation rates in high fields are not sufficiently sensitive to motions in the nanosecond frequency range. Although many proteins, and ubiquitin in particular, are mobile on slow supra-τ_c time scales (slower than overall rotational diffusion), a mere comparison of order parameters obtained from high-field relaxation and RDCs is likely to overestimate such slow motions. This study shows that high-resolution relaxometry with fast sample shuttling allows one to map the spectral density functions in exquisite detail and offers unprecedented information about local motions in proteins on time scales that are faster than or comparable to their overall tumbling.

METHODS

Magnetic Field Mapping. The magnetic field was measured as a function of the height above the magnetic center in steps of 1 mm using a homemade mapping device with two calibrated triple-axes Hall probes (Senis) with a precision of 0.1%. A CH3A10mE3D transducer was used for measurements from 0.05 to 2 T, while a 03A05F-A20T0K5Q transducer was used between 1 and 13 T.

Relaxation Experiments. The experiments were carried out on samples of 0.2 and 3 mM uniformly ^{15}N labeled human ubiquitin (Giotto) in 50 mM acetate buffer (pH 4.5) in H_2O/D_2O (90/10 v/v) at $296 \leq T \leq 297.2$ K using a 600 MHz Bruker Avance III spectrometer equipped with our pneumatic sample shuttle for measurements at low field. The pulse sequence shown in Figure 3 was used for $0.5 < B_0 < 5$ T, with a recovery delay of 2.2 s. All experiments were acquired with 16 transients and 64 complex points in the indirect t_1 dimension. Water-flip back pulses were applied to minimize the saturation of the water resonance;[59] the WATERGATE[60] scheme was used prior to detection. Frequency sign discrimination in the ω_1 domain was achieved with the States−TPPI method.[61] A full relaxation decay comprising 7−8 interleaved spectra could be recorded in 10−12 h. All signals were recorded at 14.1 T with a prototype probe equipped with z axis gradients and processed and analyzed with NMRPipe.[62] The relaxation curves at low fields were fitted to monoexponential functions.

Relaxation Data Analysis. The analysis of relaxation rates was performed with our ICARUS process, which uses ROTDIF[42] and DYNAMICS[48] at each iteration. All programs are written in Matlab (MathWorks, Inc.) A full description is given in Supporting Information. In order to account for systematic errors, a jack-knife procedure was used: the analysis was repeated seven times while excluding one of the seven low-field relaxation rates. The order parameters shown in Figure 5 result from the average over the seven analyses, and the errors correspond to the standard deviation of all seven values weighted by $6^{1/2}$.

The analysis was carried out with similar parameters as in many other NMR studies of protein dynamics. An internuclear nitrogen−hydrogen distance d_{NH} = 1.02 Å and a ^{15}N chemical shift anisotropy of −160 ppm were assumed to be common to all peptide bonds.

The effective distances between the H^N amide proton and the two additional protons are critical for scaling the corrections in the ICARUS procedure. In order to determine these distances, we measured longitudinal relaxation rates at 14.1 T with experiments similar to the shuttling method but where the longitudinal nitrogen-15 polarization is allowed to evolve during fixed intervals before and after the relaxation delay, during which no rf pulses are applied. The optimal distances d_{HH} were found to vary between 1.6 and 2.7 Å with an average of 2.1 Å. This result is confirmed by a computation of the sum of dipolar interactions with all protons (see Supporting Information) where the median value corresponds to an effective distance d_{HH} = 2.07 Å. Unfortunately, site-specific variations of d_{HH} obtained in the two approaches were only weakly correlated so that we decided to use an average d_{HH} = 2.1 Å for all residues. In order to evaluate the potential systematic errors of the resulting order parameters, we carried out a complete ICARUS analysis for a series of distances $1.7 < d_{HH} < 2.6$ Å. Results are shown in the Supporting Information. Order parameters of some sites tend to be sensitive to the distance d_{HH}, but the main features of our analysis, in particular the low order parameters found in the $\beta_1-\beta_2$ turn, remain stable regardless of the distance d_{HH}.

ASSOCIATED CONTENT

Supporting Information

Detailed presentation of the shuttle system; temperature control; description of the ICARUS protocol; results of ICARUS analysis; tables of all measured and corrected relaxation rates as well as microdynamic parameters obtained from analysis of relaxation at 14.1 T only, three high fields, and all 10 fields. This material is available free of charge via the Internet at http://pubs.acs.org.

AUTHOR INFORMATION

Corresponding Author

Fabien.Ferrage@ens.fr

Author Contributions

$^{\perp}$C.C. and S.N.K. contributed equally.

Notes

The authors declare the following competing financial interest(s): T.M., V.R., and F.E. are employees of Bruker Biospin. The authors declare no other competing financial interest.

■ ACKNOWLEDGMENTS

The authors thank A. Guiga (CEA) for machining the field-mapping device; Martin Blackledge (IBS, Grenoble), Arthur G. Palmer (Columbia University), Daniel Abergel (ENS), and Pau Bernado (CBS, Montpellier) for fruitful exchanges; Martin Blackledge for sharing data; and Daniel Abergel and Martin Blackledge for carefully reading the manuscript. We thank Philip Lottmann and Christian Griesinger (Max Planck Institute, Göttingen) for their contributions to the shuttle design as well as Nelly Morellet (ICSN, Gif-sur-Yvette) for assistance with high-field spectrometers. This research has received funding from the European Research Council (ERC) under the European Community's Seventh Framework Programme (FP7/2007-2013), ERC Grant 205119 (REvolutioNMR) to D.S. and Grant 279519 (2F4BIODYN) to F.F., as well as from the Agence Nationale de la Recherche (ANR-11-BS07-031-01). Financial support from the TGIR-RMN-THC Fr3050 CNRS is gratefully acknowledged.

■ REFERENCES

(1) Palmer, A. G. *Chem. Rev.* **2004**, *104*, 3623.
(2) Peng, J. W.; Wagner, G. *J. Magn. Reson.* **1992**, *98*, 308.
(3) Prompers, J. J.; Bruschweiler, R. *J. Am. Chem. Soc.* **2002**, *124*, 4522.
(4) Lipari, G.; Szabo, A. *J. Am. Chem. Soc.* **1982**, *104*, 4546.
(5) Clore, G. M.; Szabo, A.; Bax, A.; Kay, L. E.; Driscoll, P. C.; Gronenborn, A. M. *J. Am. Chem. Soc.* **1990**, *112*, 4989.
(6) Calligari, P.; Calandrini, V.; Kneller, G. R.; Abergel, D. *J. Phys. Chem. B* **2011**, *115*, 12370.
(7) Ochsenbein, F.; Neumann, J. M.; Guittet, E.; Van Heijenoort, C. *Protein Sci.* **2002**, *11*, 957.
(8) Buevich, A. V.; Baum, J. *J. Am. Chem. Soc.* **1999**, *121*, 8671.
(9) Tugarinov, V.; Liang, Z. C.; Shapiro, Y. E.; Freed, J. H.; Meirovitch, E. *J. Am. Chem. Soc.* **2001**, *123*, 3055.
(10) Luchinat, C.; Parigi, G. *J. Am. Chem. Soc.* **2007**, *129*, 1055.
(11) Persson, E.; Halle, B. *J. Am. Chem. Soc.* **2008**, *130*, 1774.
(12) (a) Redfield, A. G. *Magn. Reson. Chem.* **2003**, *41*, 753. (b) Redfield, A. G. *J. Biomol. NMR* **2012**, *52*, 159.
(13) Victor, K.; Kavolius, V.; Bryant, R. G. *J. Magn. Reson.* **2004**, *171*, 253.
(14) Chou, C. Y.; Chu, M. L.; Chang, C. F.; Huang, T. H. *J. Magn. Reson.* **2012**, *214*, 302.
(15) Roberts, M. F.; Redfield, A. G. *Proc. Natl. Acad. Sci. U.S.A.* **2004**, *101*, 17066.
(16) Clarkson, M. W.; Lei, M.; Eisenmesser, E. Z.; Labeikovsky, W.; Redfield, A.; Kern, D. *J. Biomol. NMR* **2009**, *45*, 217.
(17) Dikic, I.; Wakatsuki, S.; Walters, K. J. *Nat. Rev. Mol. Cell Biol.* **2009**, *10*, 659.
(18) Zhang, Y. N.; Zhou, L. J.; Rouge, L.; Phillips, A. H.; Lam, C.; Liu, P.; Sandoval, W.; Helgason, E.; Murray, J. M.; Wertz, I. E.; Corn, J. E. *Nat. Chem. Biol.* **2013**, *9*, 51.
(19) Lange, O. F.; Lakomek, N. A.; Fares, C.; Schroder, G. F.; Walter, K. F. A.; Becker, S.; Meiler, J.; Grubmuller, H.; Griesinger, C.; de Groot, B. L. *Science* **2008**, *320*, 1471.
(20) Miloushev, V. Z.; Levine, J. A.; Arbing, M. A.; Hunt, J. F.; Pitt, G. S.; Palmer, A. G. *J. Biol. Chem.* **2009**, *284*, 6446.
(21) Massi, F.; Grey, M. J.; Palmer, A. G., III. *Protein Sci.* **2005**, *14*, 735.
(22) Ban, D.; Funk, M.; Gulich, R.; Egger, D.; Sabo, T. M.; Walter, K. F. A.; Fenwick, R. B.; Giller, K.; Pichierri, F.; de Groot, B. L.; Lange, O. F.; Grubmüller, H.; Salvatella, X.; Wolf, M.; Loidl, A.; Kree, R.; Becker, S.; Lakomek, N.-A.; Lee, D.; Lunkenheimer, P.; Griesinger, C. *Angew. Chem., Int. Ed.* **2011**, *50*, 11437.
(23) Salvi, N.; Ulzega, S.; Ferrage, F.; Bodenhausen, G. *J. Am. Chem. Soc.* **2012**, *134*, 2481.
(24) Tollinger, M.; Sivertsen, A. C.; Meier, B. H.; Ernst, M.; Schanda, P. *J. Am. Chem. Soc.* **2012**, *134*, 14800.
(25) Ban, D.; Gossert, A. D.; Giller, K.; Becker, S.; Griesinger, C.; Lee, D. *J. Magn. Reson.* **2012**, *221*, 1.
(26) Briggman, K. B.; Tolman, J. R. *J. Am. Chem. Soc.* **2003**, *125*, 10164.
(27) Peti, W.; Meiler, J.; Brüschweiler, R.; Griesinger, C. *J. Am. Chem. Soc.* **2002**, *124*, 5822.
(28) Lakomek, N. A.; Walter, K. F. A.; Fares, C.; Lange, O. F.; de Groot, B. L.; Grubmuller, H.; Bruschweiler, R.; Munk, A.; Becker, S.; Meiler, J.; Griesinger, C. *J. Biomol. NMR* **2008**, *41*, 139.
(29) Salmon, L.; Bouvignies, G.; Markwick, P.; Lakomek, N.; Showalter, S.; Li, D. W.; Walter, K.; Griesinger, C.; Bruschweiler, R.; Blackledge, M. *Angew. Chem., Int. Ed.* **2009**, *48*, 4154.
(30) Salmon, L.; Bouvignies, G.; Markwick, P.; Blackledge, M. *Biochemistry* **2011**, *50*, 2735.
(31) Lienin, S. F.; Bremi, T.; Brutscher, B.; Brüschweiler, R.; Ernst, R. R. *J. Am. Chem. Soc.* **1998**, *120*, 9870.
(32) Tjandra, N.; Feller, S. E.; Pastor, R. W.; Bax, A. *J. Am. Chem. Soc.* **1995**, *117*, 12562.
(33) Chang, S. L.; Tjandra, N. *J. Magn. Reson.* **2005**, *174*, 43.
(34) Ferrage, F.; Pelupessy, P.; Cowburn, D.; Bodenhausen, G. *J. Am. Chem. Soc.* **2006**, *128*, 11072.
(35) Reese, M.; Turke, M. T.; Tkach, I.; Parigi, G.; Luchinat, C.; Marquardsen, T.; Tavernier, A.; Hofer, P.; Engelke, F.; Griesinger, C.; Bennati, M. *J. Am. Chem. Soc.* **2009**, *131*, 15086.
(36) Morris, G. A.; Freeman, R. *J. Am. Chem. Soc.* **1979**, *101*, 760.
(37) Burum, D. P.; Ernst, R. R. *J. Magn. Reson.* **1980**, *39*, 163.
(38) Pelupessy, P.; Espallargas, G. M.; Bodenhausen, G. *J. Magn. Reson.* **2003**, *161*, 258.
(39) Pelupessy, P.; Ferrage, F.; Bodenhausen, G. *J. Chem. Phys.* **2007**, *126*, 134508.
(40) Ferrage, F.; Cowburn, D.; Ghose, R. *J. Am. Chem. Soc.* **2009**, *131*, 6048.
(41) Ferrage, F.; Reichel, A.; Battacharya, S.; Cowburn, D.; Ghose, R. *J. Magn. Reson.* **2010**, *207*, 294.
(42) Walker, O.; Varadan, R.; Fushman, D. *J. Magn. Reson.* **2004**, *168*, 336.
(43) Cornilescu, G.; Marquardt, J. L.; Ottiger, M.; Bax, A. *J. Am. Chem. Soc.* **1998**, *120*, 6836.
(44) Liu, Z.; Zhang, W. P.; Xing, Q.; Ren, X. F.; Liu, M. L.; Tang, C. *Angew. Chem., Int. Ed.* **2012**, *51*, 469.
(45) Ryabov, Y. E.; Fushman, D. *J. Am. Chem. Soc.* **2007**, *129*, 3315.
(46) Kay, L. E.; Nicholson, L. K.; Delaglio, F.; Bax, A.; Torchia, D. A. *J. Magn. Reson.* **1992**, *97*, 359.
(47) Palmer, A. G., III; Skelton, N. J.; Chazin, W. J.; Wright, P. E.; Rance, M. *Mol. Phys.* **1992**, *75*, 699.
(48) Fushman, D.; Cahill, S.; Cowburn, D. *J. Mol. Biol.* **1997**, *266*, 173.
(49) Showalter, S. A.; Bruschweiler, R. *J. Chem. Theory Comput.* **2007**, *3*, 961.
(50) Maragakis, P.; Lindorff-Larsen, K.; Eastwood, M. P.; Dror, R. O.; Klepeis, J. L.; Arkin, I. T.; Jensen, M. O.; Xu, H. F.; Trbovic, N.; Friesner, R. A.; Palmer, A. G.; Shaw, D. E. *J. Phys. Chem. B* **2008**, *112*, 6155.
(51) Markwick, P. R. L.; Bouvignies, G.; Salmon, L.; McCammon, J. A.; Nilges, M.; Blackledge, M. *J. Am. Chem. Soc.* **2009**, *131*, 16968.
(52) Fenwick, R. B.; Esteban-Martin, S.; Richter, B.; Lee, D.; Walter, K. F. A.; Milovanovic, D.; Becker, S.; Lakomek, N. A.; Griesinger, C.; Salvatella, X. *J. Am. Chem. Soc.* **2011**, *133*, 10336.
(53) Long, D.; Brüschweiler, R. *PLoS Comput. Biol.* **2011**, *7*, e1002035.
(54) Bouvignies, G.; Bernado, P.; Meier, S.; Cho, K.; Grzesiek, S.; Bruschweiler, R.; Blackledge, M. *Proc. Natl. Acad. Sci. U.S.A.* **2005**, *102*, 13885.
(55) Henzler-Wildman, K. A.; Lei, M.; Thai, V.; Kerns, S. J.; Karplus, M.; Kern, D. *Nature* **2007**, *450*, 913.
(56) Kroenke, C. D.; Loria, J. P.; Lee, L. K.; Rance, M.; Palmer, A. G., III. *J. Am. Chem. Soc.* **1998**, *120*, 7905.
(57) Wong, V.; Case, D. A.; Szabo, A. *Proc. Natl. Acad. Sci. U.S.A.* **2009**, *106*, 11016.

(58) Ryabov, Y.; Clore, G. M.; Schwieters, C. D. *J. Chem. Phys.* **2012**, *136*, 034108.
(59) Grzesiek, S.; Bax, A. *J. Am. Chem. Soc.* **1993**, *115*, 12593.
(60) Piotto, M.; Saudek, V.; Sklenar, V. *J. Biomol. NMR* **1992**, *2*, 661.
(61) Marion, D.; Ikura, M.; Tschudin, R.; Bax, A. *J. Magn. Reson.* **1989**, *85*, 393.
(62) Delaglio, F.; Grzesiek, S.; Vuister, G. W.; Zhu, G.; Pfeifer, J.; Bax, A. *J. Biomol. NMR* **1995**, *6*, 277.